Effects of phosphonium-based ionic liquids on phospholipid membranes studied by small-angle X-ray scattering

Kontro, Inkeri

2016-12

Kontro , I , Svedström , K , Dusa , F , Ahvenainen , P , Ruokonen , S-K , Witos , J & Wiedmer , S K 2016 , ' Effects of phosphonium-based ionic liquids on phospholipid membranes studied by small-angle X-ray scattering ' , Chemistry and Physics of Lipids , vol. 201 , pp. 59-66 . https://doi.org/10.1016/j.chemphyslip.2016.11.003

http://hdl.handle.net/10138/174146
https://doi.org/10.1016/j.chemphyslip.2016.11.003

acceptedVersion

Effects of phosphonium-based ionic liquids on phospholipid membranes studied by small-angle X-ray scattering

Inkeri Kontro[a], Kirsi Svedström[a], Filip Duša[b,c], Patrik Ahvenainen[a], Suvi-Katriina Ruokonen[b], Joanna Witos[b], Susanne K. Wiedmer[b]

a) Department of Physics, P.O.B. 64, 00014 University of Helsinki, Finland

b) Department of Chemistry, P.O.B. 55, 00014 University of Helsinki, Finland

c) Institute of Analytical Chemistry of the CAS, v. v. i., Brno, Czech Republic

Abstract

The effects of ionic liquids on model phospholipid membranes were studied by small-angle X-ray scattering, dynamic light scattering (DLS) and zeta potential measurements. Multilamellar 1-palmitoyl-2-oleoyl-*sn*-glycero-3-phosphocholine liposomes and large unilamellar vesicles composed of L-α-phosphatidylcholine (eggPC) and L-α-phosphatidylglycerol (eggPG) (80:20 mol%) or eggPC, eggPG, and cholesterol (60:20:20 mol%) were used as biomimicking membrane models. The effects of the phosphonium-based ionic liquids: tributylmethylphosphonium acetate, trioctylmethylphosphonium acetate, tributyl(tetradecyl)-phosphonium acetate, and tributyl(tetradecyl)-phosphonium chloride, were compared to those of 1-ethyl-3-methyl-imidazolium acetate. With multilamellar vesicles, the ionic liquids that did not disrupt liposomes decreased the lamellar spacing as a function of concentration. The magnitude of the effect depended on concentration for all studied ionic liquids. Using large unilamellar vesicles, first a slight decrease in the vesicle size, then aggregation of vesicles was observed by DLS for increasing ionic liquid concentrations. At concentrations just below those that caused aggregation of liposomes, large unilamellar vesicles were coated by ionic liquid cations, evidenced by a change in their zeta potential. The ability of phosphonium-based ionic liquids to affect liposomes is related to the length of the hydrocarbon chains in the cation. Generally, the ability of ionic liquids to disrupt liposomes goes hand in hand with inducing disorder in the phospholipid membrane. However, trioctylmethylphosphonium acetate selectively extracted and induced a well-ordered lamellar structure in phospholipids from disrupted cholesterol-containing large unilamellar vesicles. This kind of effect was not seen with any other combination of ionic liquids and liposomes.

1 Introduction

The outer boundary of cells, the cell membrane, is composed of a lipid bilayer which acts both as a physical boundary, offers protection from the environment, and offers a platform for surface structures and *e.g.* membrane proteins. While cell membranes are usually composed of a complex mixture of lipids, they can be mimicked by the self-assembly of suitable phospholipids in aqueous solutions. When dry phospholipids are

hydrated, they form multilamellar vesicles, but unilamellar biomimicking vesicles can be formed by for example extrusion.

Crossing of the lipid bilayer of the cell membrane is not the only or often even primary path for molecule penetrations into the cell. In many cases, however, the effects of the molecules on the cell membrane have an impact on the whole cell. For example, the toxic effects of ionic liquids (ILs) have primarily been linked to their effects on cell membranes (Stolte et al., 2007). ILs are salts, which are liquid at room temperature, and due to the nearly endless combinations of anions and cations available, the solvent properties of ILs are highly tunable. The IL toxicity increases with increasing lipophilicity (Ranke et al., 2007) and thereby length of the lipophilic cationic groups (Mikkola et al., 2015). However, the type of anion also plays a role, particularly for bulky anions with long and/or branched alkyl chains (Egorova and Ananikov, 2014; Petkovic et al., 2010; Ruokonen et al., 2016). The resulting effect is therefore a combination of the properties of the anion and cation.

ILs display many properties desirable for solvents: they dissolve biomass, are of low volatility, and are thermally and chemically highly stable. ILs have been considered as designer "green" solvents which can be utilized for solving many problems encountered with the widespread use of volatile organic solvents (Earle and Seddon, 2000). New uses for ILs include cellulose regeneration (Zhu et al., 2006), as electrolytes in fuel cells (Diaz et al., 2014) and organic and nanoparticle syntheses (Antonietti et al., 2004). Common ILs include imidazolium moieties, but many other possibilities exist. While some ILs are well tolerated by e.g. fungi (Petkovic et al., 2010), many ILs have been shown to be toxic towards microbes (Docherty and Kulpa, 2005), algae, invertebrates and vertebrates (Pretti et al., 2009), and other environmental concerns are related to their stability and low (bio)degradability (Thi et al., 2010).

Phosphonium-based ILs are quaternary phosphonium salts that, although less studied than the more common nitrogen-based ILs, have recently become available in industrial scale. Phosphonium-based ILs are in some ways preferable to their nitrogen-based counterparts: they have a higher thermal stability and they tend to be less acidic than their imidazolium cation analogues (Fraser and MacFarlane, 2009). However, phosphonium-based ILs are generally more toxic than other moieties (Egorova and Ananikov, 2014). As few studies have looked at the effects of phosphonium-based ILs, there is a clear need for more studies on this topic.

In a previous study (Mikkola et al., 2015), the length of the longest hydrocarbon chain of the IL influenced the toxicity of phosphonium-based ILs, with the long (14-carbon) chains being highly harmful and the shorter (4 to 8 carbons) chains significantly less harmful. The toxicity results from human corneal epithelial cells and

E. coli cells correlated with changes in the liposome surface charge and shape, indicating that the cytotoxicity is in part due to interactions between the ILs and the phospholipid bilayer. The concentration at which ILs start to form micelles (critical micelle concentration, CMC) correlates well with the concentration at which the ILs start to disrupt unilamellar vesicles (LUV) (Dusa et al., 2015; Ruokonen et al., 2016). Clearly, the effects of ILs on lipid bilayers are more destructive at concentrations where IL micelles form.

However, there are few methods to directly access the dynamics of biomembranes. A way forward is to use simple analogues for complex membranes, such as phospholipid supported multilayers (e.g. organized lamellae), multilamellar vesicles (MLVs) or LUV composed of one or more lipid species. While LUVs are better mimics of biological systems, many methods are more suited for multilamellar samples, thus also MLVs are widely used for *e.g.* in computational studies and in X-ray and neutron scattering studies.

These biomimetic systems and their reactions with ILs are probed by *e.g.* computational means (Benedetto et al., 2015; Cromie et al., 2009; Yoo et al., 2016), although the size of the sample may currently be too limited for all effects to show in computations (Benedetto and Ballone, 2015). Also physical probes, such as neutron reflectometry (Benedetto et al., 2014), fluorescent microscopy (Yoo et al., 2016), or small-angle X-ray scattering (SAXS) (Jing et al., 2016), have been used. For example, the effects of two commonly used ILs, 1-butyl-3-methyl-imidazolium chloride and choline chloride, on model membranes composed of 1-palmitoyl-2-oleyl-*sn*-glycero-3-phosphocholine (POPC) and 1,2-dimyristoyl-*sn*-glycero-3-phosphatidylcholine, have been studied by neutron reflectometry to provide insight into the penetration of the ILs into the lipid bilayer (Benedetto et al., 2014). At all studied concentrations, the lipid bilayers shrunk in thickness by ~0.1 nm due to the IL cations penetrating into the lipid bilayers. The IL amount immobilized into the bilayer was dependent on the lipid species, however, independent of the type of IL. Neutrons are very sensitive to phospholipids due to the large amount of hydrogen atoms in the hydrocarbon tails of the lipids. Deuteration of the sample offers a way to further pinpoint the reflecting structures, but the disadvantages of neutrons are lower flux and thus longer measurement times compared to X-rays.

SAXS is a technique where incoming monochromatic X-rays are scattered from inhomogeneities in the electron density of a sample. This technique provides a scattering average from a sample, typically a few microliters in volume. With high-flux sources such as synchrotrons, the SAXS experiments are quick, with measurement times from a few minutes down to microseconds for high-brilliance beamlines. In the case of MLVs with well-ordered lamellae, the SAXS pattern consists of well-defined diffraction peaks, which can easily be determined. For LUVs, the characteristic SAXS patterns can be interpreted using modelling of the electron densities of the bilayers (see *e.g.* (Pabst et al., 2010; Varga et al., 2014)).

In this study, we used SAXS to study well-ordered phosphatidyl choline MLVs exposed to phosphonium-based ILs. In addition, we used dynamic light scattering (DLS) and zeta potential measurements to study LUVs exposed to the same ILs. These LUV results are complemented by preliminary SAXS results. The LUVs were composed of L-α-phosphatidylcholine and L-α-phosphatidylglycerol (80:20 mol%) or L-α-phosphatidylcholine, L-α-phosphatidylglycerol and cholesterol (60:20:20 mol%). Cholesterol was included in the LUVs because cholesterol is a common membrane component in eukaryotic organisms: it comprises 20 wt-% in human red blood cells (Lemmich et al., 1997) and over 50 wt-% of lipids in cornea (Gaynor et al., 1996). Cholesterol is known to affect the rigidity of the lipid membranes by increasing the order of the phospholipid chains (Mannock et al., 2010).

The ILs studied are tributylmethylphosphonium acetate [P_{4441}][OAc], trioctylmethylphosphonium acetate ([P_{8881}][OAc]), tributyl(tetradecyl)phosphonium acetate and the corresponding chloride ([P_{14444}][OAc] and [P_{14444}]Cl respectively), as well as imidazolium-based 1-ethyl-3-methylimidazolium acetate ([emim][OAc]). For the ILs having a CMC point, one concentration below or around and one above it were used, except for [P_{8881}][OAc], for which two concentrations above the CMC point were used. ILs with alkyl chains with four or fewer carbons are not expected to have a CMC (Blesic et al., 2007; Chen et al., 2014). [emim][OAc] is used here as a reference due to its known low toxicity and the widespread use of imidazolium-based ILs.

2 Experimental

2.1 Liposome preparation

1-Palmitoyl-2-oleoyl-*sn*-glycero-3-phosphocholine (sodium salt) (POPC), L-α-phosphatidylcholine (egg, chicken) (sodium salt) (eggPC), L-α-phosphatidylglycerol (egg, chicken) (sodium salt) (eggPG), and cholesterol were purchased from Avanti Lipids (Alabaster, AL, USA). Chloroform was used as a solvent for lipid stock solutions in all cases. MLV POPC samples were prepared from 20 mM POPC stock solution. The chloroform was evaporated under a stream of pressurized air and the solvent residues were removed by keeping the samples under reduced pressure overnight. The lipids were hydrated with sodium phosphate buffer (pH = 7.4, I = 10 mM) to a concentration of 5 mM total lipids. The dispersions were kept at 60 °C under agitation for 1 h. For large unilamellar vesicles, a 20 mM stock solution of eggPC and a 10 mM stock solution of eggPG (80:20 mol%) or aforementioned eggPC and eggPG stock solutions and a 8.32 mM stock solution of cholesterol (60:20:20 mol%) were combined. The samples were prepared as MLV samples for SAXS experiments. After agitation, the samples were sonicated at 37 kHz for 10 min at full (100%) power in Elmasonic P 30 H (Elma GmbH & Co KG, Singen, Germany). The tank was filled to half of its volume with a mix of ice and chilled water in a ratio of approximately 1:1. For DLS and zeta potential experiments, the samples

were hydrated with MilliQ water instead of sodium phosphate buffer. The LUVs were prepared by extrusion (21 times) through 100 nm membranes at room temperature.

2.2 Ionic liquids

Tributyl(tetradecyl)phosphonium acetate ([P_{14444}][OAc]; M=458.7 g·mol^{-1}) was synthesized by anion metathesis as described in previous articles (Holding et al., 2014; Mikkola et al., 2015). Trioctylmethylphosphonium acetate ([P_{8881}][OAc]; M=445.9 g·mol^{-1}) was synthesized as described previously in (Holding et al., 2014; Labafzadeh et al., 2015). Tributyl(tetradecyl)phosphonium chloride ([P_{14444}]Cl; M=435.2 g·mol^{-1}) was provided by Cytec Industries (Woodland Park, NJ). Methyltributylphosphonium acetate ([P_{4441}][OAc]; M=264.3 g·mol^{-1}), was synthesized as described in our previous article (Ruokonen et al., 2016). 1-Ethyl-3-methylimidazolium acetate ([emim][OAc]; M=146.6 g·mol^{-1}) and tributylmethylphosphonium methyl carbonate solution (purity >95%, 80% w/v in methanol) were purchased from IoLiTec GmbH (Heilbronn, Germany). The IL cations and anions are presented in Supporting information (Figure S1).

2.3 SAXS measurements

The measurements were performed on beamline I911-SAXS at Max IV Laboratory, Lund, Sweden. The flow-through capillary system of the beamline was used (Labrador et al., 2013). The wavelength of the incident radiation was λ = 0.091 nm. Calibration was done with a silver behenate sample to obtain a q-scale of 0.094 nm$^{-1} \leq q \leq$ 4.39 nm^{-1}, where $q = 4\pi \sin\theta / \lambda$ is the length of the scattering vector and θ is half of the scattering angle 2θ. Absorption correction was applied, and no other corrections were made for the data. As the data were not corrected for the buffer background, all SAXS results presented and discussed here are carefully chosen so that the background does not have an effect on them. Each data set represents an average of 2 to 10 one-minute measurements. Single one-minute measurements are presented when time-dependent processes are discussed.

IL stock solutions in sodium phosphate buffer were mixed with liposome samples immediately before SAXS experiments to a final lipid concentration of 4 mM. IL concentrations were chosen around and above the CMC (for the ILs expected to have a CMC value). Determination of the CMC of [P_{8881}][OAc] is discussed in Supporting information (Section 2).

The positions of diffraction peaks were determined by fitting a pseudo-Voigt peak profile into the data, and the lamellar distance d was calculated as $d = 2\pi/q$. The fits were repeated for 1000 simulated data sets obtained by the Monte Carlo method from the observed scattering intensities and their uncertainties, and uncertainties of the peak position, full width at half maximum (FWHM) and lamellar distance were derived

from standard deviations of the fits. The length of the scattering region, s, was estimated from the well-known Scherrer equation:

$$s = \frac{K\lambda}{\beta \cos\theta}, \quad (1)$$

where K = 0.9 is a structure coefficient, λ the incident wavelength, β the FWHM of the peak in radians, and θ half of the scattering angle corresponding to the peak position.

2.4 DLS and zeta potential measurements

The size distribution and zeta potential of LUVs were measured using Zetasizer Nano-ZS (Malvern Instruments Ltd, Worcestershire, UK). The liposomes were diluted to 0.1 mM concentration. DLS measurements were conducted at 20 °C using a helium-neon laser at 633 nm, detection angle of 173°, and a viscosity value of 1.0031 cP (for water). Measurements were repeated three times and an average intensity was calculated. Zeta potential measurements were conducted at 20 °C, and a dielectric constant of 80.4 (for water) and a viscosity value of 1.0031 cP (for water) were used in the calculations. The applied electric field strength was 150 V·cm^{-1}. One run consisted of ten individual measurements and the average of three runs was calculated.

3 Results and discussion

3.1 Multilamellar vesicles

In the SAXS experiments, the reference POPC MLVs displayed two clear diffraction peaks resulting from the coherent scattering of the lipid bilayer lamellae at q = 0.974 nm^{-1} and q = 1.95 nm^{-1}, both corresponding to a lamellar spacing of 6.45 nm. The SAXS patterns of MLVs exposed to [emim][OAc] and [P_{4441}][OAc] are shown in Figure 1 and those of MLVs exposed to [P_{8881}][OAc] and [P_{14444}][OAc] are shown in Figure 2. With [emim][OAc] and [P_{4441}][OAc] no disordering of the lamellae was observed even at high concentrations (50 mM and 30 mM respectively), but addition of ILs decreased the lamellar distance. A trend is evident in Figure 1, where the diffraction peaks of the MLVs are shifted towards higher q-values as a function of IL concentration. The lamellar distances for POPC MLVs with [emim][OAc], [P_{4441}][OAc], [P_{8881}][OAc], and [P_{14444}][OAc] are listed in Table 1 as a function of IL concentrations studied.

Low concentrations (0.4-0.8 mM) of the longer chained ILs [P_{8881}][OAc] and [P_{14444}][OAc] also slightly shrunk the lamellar distance. These concentrations are below or around the CMC values of these ILs. The CMC of [P_{14444}]Cl is 0.54-0.60 mM (Dusa et al., 2015) and that of [P_{14444}][OAc] is 0.89 mM in water and 0.32 mM in

sodium phosphate buffer (pH 7.4; ionic strength 10 mM) (Ruokonen et al., 2016). For $[P_{8881}][OAc]$, the CMC is 1.43 mM in phosphate buffer (pH 7.4; ionic strength 10 mM) (see Supporting information).

While the intensity of the diffraction peaks remained the same or increased for the less-harmful ILs, addition of $[P_{8881}][OAc]$ and $[P_{14444}][OAc]$ resulted in a decrease of the intensity, as seen when comparing the intensities of the first and second diffraction peak to the reference. Despite this, the size of the scattering region (the correlation length in the direction of membrane normal), as determined from the FWHM of these peaks, changed only little in all the samples. As these ILs disrupt unilamellar vesicles at these concentration (see below and *e.g.* (Mikkola et al., 2015)), the most probable explanation for the decrease of the intensity is that the amount of well-ordered lamellae in the MLV sample decreases, *i.e.* ILs which disrupt LUVs cause disorder in MLVs. It is likely that this disorder, seen from the decrease in the intensity of diffraction peaks, is accompanied by a disruption of the liposomes as in LUVs. Additionally, the SAXS pattern of MLVs exposed to 0.4 mM $[P_{14444}][OAc]$ shows a small peak before the first MLV peak (marked with an arrow in Figure 2). The lamellar distance corresponding to the *q*-value of the new peak is 10.4 nm. Hence, already at this lower concentration, there are indications of a change in the organization of the lipids. This weak peak was not present in the sample of higher concentration of $[P_{14444}][OAc]$.

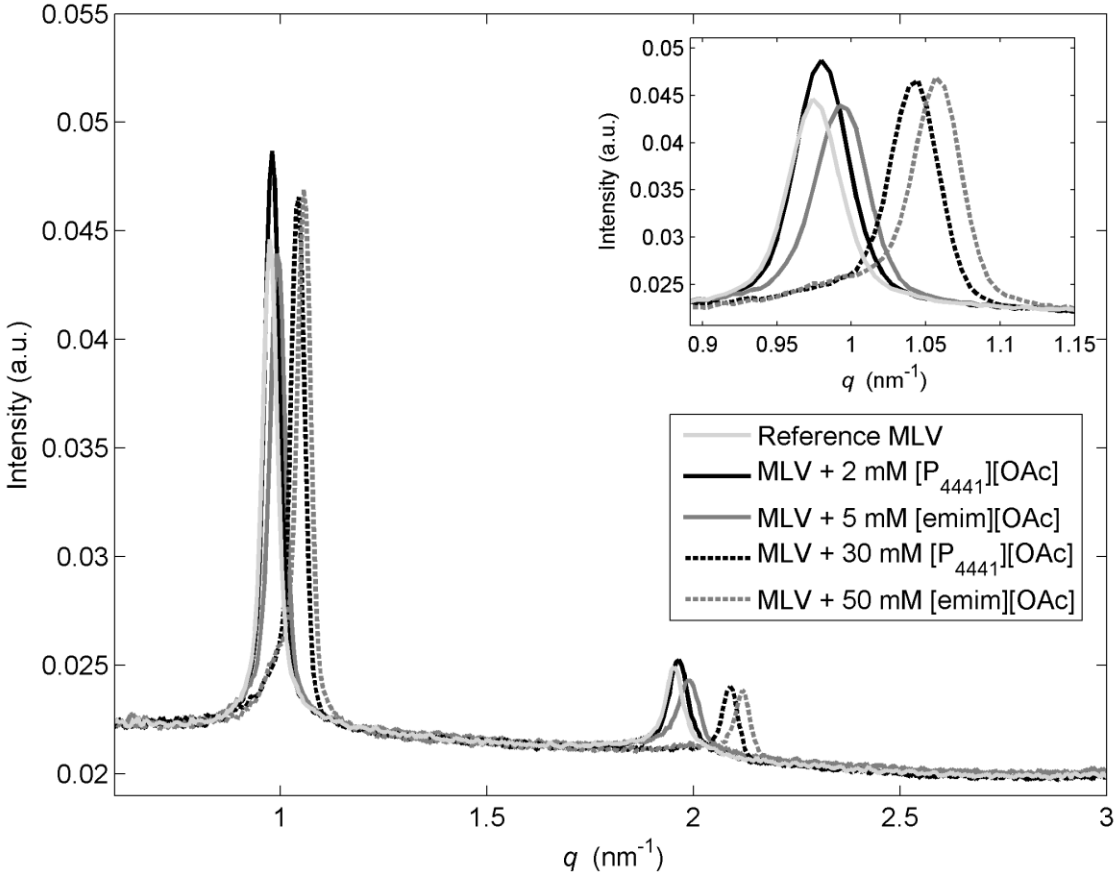

Figure 1. The effect of less harmful ionic liquids on the SAXS pattern of multilamellar POPC vesicles. Reference MLV (light gray), MLV treated with [P_{4441}][OAc] (black), and MLV treated with [emim][OAc] (dark gray). Insert: magnification of the first diffraction peak.

Since we cannot determine the instrumental broadening of β, using the Scherrer equation (Equation 1) to calculate the sizes of the scattering regions is not optimal here. Also it must be noted that in the case of lipid bilayers, an important factor for the peak broadening is the inherent disorder and fluctuation of lipids and bending of bilayers. However, as the peak width is inversely related to the size of the ordered domain, a lower limit for scattering domain size can be calculated using the determined FWHMs (Mills et al., 2008). For the samples, where FWHM could be reliably determined, the length of the scattering region (*s*) was 190-210 nm. This corresponds to ~30 multilayers for all samples where both peak position and width could be determined. Thus, even when the phospholipid samples are losing order and dissolving, a long-range order remains in parts of the sample. Also, the almost constant width of the first diffraction peak from sample to sample indicates that the properties are the same throughout the sample, and the IL effect on the outer lamellae is the same as that on the inner lamellae of the MLV. Varying properties of the lamellae throughout the sample would result in one or some of the following: secondary diffraction peaks corresponding to a secondary lamellar spacing, deformed diffraction peaks resulting from the overlap of two or more diffraction

peaks, or widened diffraction peaks due to the reduced size of the scattering region. With the exception of the MLVs mixed with 0.4 mM $[P_{14444}][OAc]$, where a small, new diffraction peak is present, no features indicating different kinds of lamellar order in the sample are present. This is a common feature observed both for harmful and less-harmful ILs and indicates that all studied ILs are able to pass through the MLV membrane.

At higher concentrations (3.0-16.8 mM), the effects of $[P_{8881}][OAc]$ and $[P_{14444}][OAc]$ clearly differed from those of the less harmful [emim][OAc] and $[P_{4441}][OAc]$. As seen in Figure 2, at these higher concentrations of the longer-chained IL cations, MLV structures declined rapidly. For the sample treated with $[P_{14444}][OAc]$, a rapid decline of lamellar structure was observed at 3 mM concentration although a vague maximum centered around q = 1 nm^{-1} remained. This indicates that the structure with certain correlation lengths still remains in the sample, even though the ordered lamellar structure has disappeared. The new structure corresponds to larger real space distances than those present in the reference LUVs (see Figure 3 and Supporting information, Figures S6-S7), as the maximum is at lower q-values.

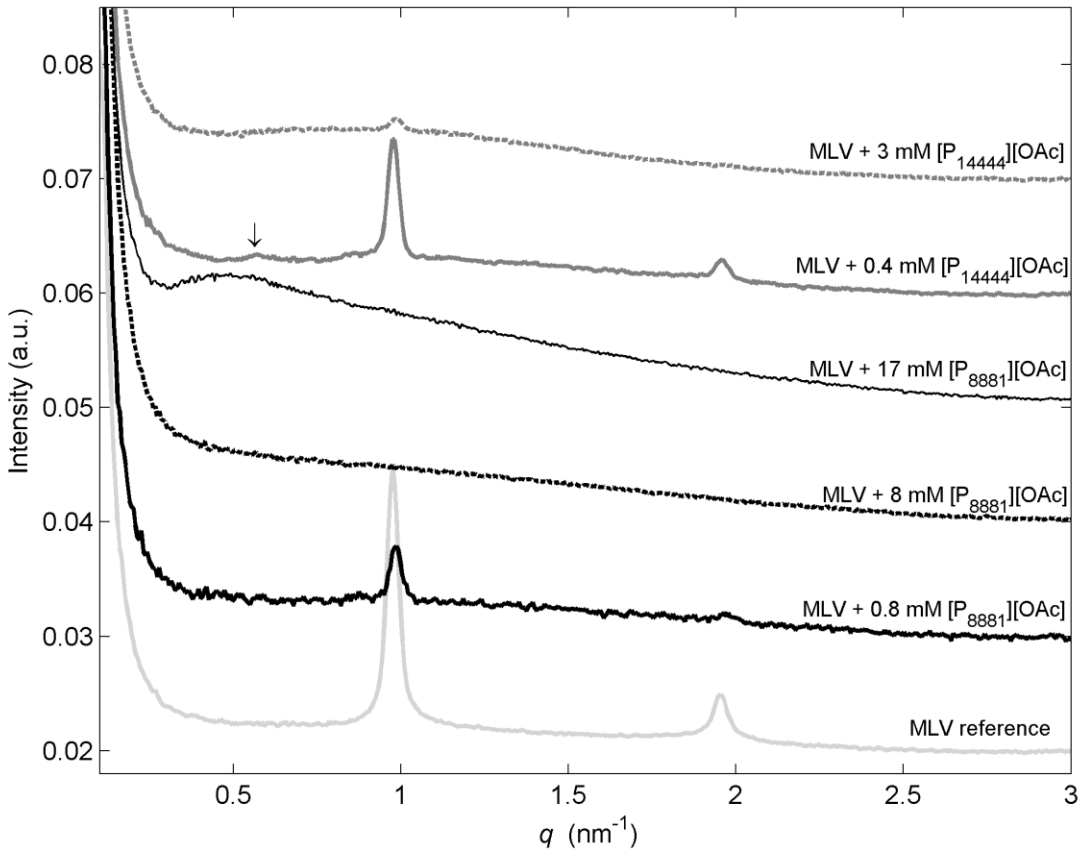

Figure 2. The effect of highly harmful ionic liquids on the SAXS pattern of multilamellar POPC vesicles. Reference MLV (light gray), MLV with $[P_{8881}][OAc]$ (black) and $[P_{14444}][OAc]$ (dark gray). The arrow marks the position of a new peak.

Neither diffraction peaks nor a similar wide and vague maximum remained in the phospholipid sample exposed to 8 mM [P_{8881}][OAc] (Figure 2). At this concentration, the SAXS pattern of the sample is flat, indicating a high state of disorder in the sample: the POPC molecules have lost their ability to aggregate into any kind of ordered structure. When the concentration of [P_{8881}][OAc] was further increased to 17 mM, a new, asymmetric halo appeared at q = 0.5 nm^{-1}. As a lower q-value is associated with a larger real-space distance, this indicates that the resulting structure has electron density fluctuations in a larger size-scale than the reference liposomes. While this IL itself (17 mM [P_{8881}][OAc]) also causes a SAXS signal that differs from the buffer scattering (Supplementary information, Figure S4), this scattering is weaker than that of liposomes or the IL-lipid complexes that form. The scattering from other ILs or [P_{8881}][OAc] at a lower concentration does not significantly differ from that of the buffer.

*Table 1. Effect of ionic liquids on POPC MLV lamellar distance. * no peaks, ** peaks rapidly declining during measurement.*

Ionic liquid	conc (mM)	peak position (nm^{-1})	lamellar distance (nm)	peak FWHM (nm^{-1})
none	-	0.975 ± 0.001	6.44 ± 0.01	0.026 ± 0.003
[emim][OAc] CMC > 50.0 mM	5.0	0.993 ± 0.001	6.33 ± 0.01	0.028 ± 0.003
	50.0	1.057 ± 0.001	5.94 ± 0.01	0.025 ± 0.004
$[P_{4441}][OAc]$ CMC > 30.0 mM	2.0	0.980 ± 0.001	6.41 ± 0.01	0.027 ± 0.004
	30.0	1.042 ± 0.001	6.04 ± 0.01	0.025 ± 0.004
$[P_{8881}][OAc]$ CMC = 1.43 mM±0.09 mM (in buffer pH 7.4), 2.16±0.28 mM (in H_2O)	0.8	0.983 ± 0.001**	6.39 ± 0.03	0.027 ± 0.005
	8.0	*	-	-
	16.8	*	-	-
$[P_{14444}][OAc]$ CMC = 0.32 mM	0.4	0.977 ± 0.001	6.43 ± 0.04	0.025 ± 0.004
	3.0	0.984 ± 0.001**	6.38 ± 0.07	-

The effects of ILs on well-ordered lipid bilayer lamellae are thus two-fold. Completely destroyed lamellar structures were observed, and in the samples where the liposomes were not otherwise affected by the addition of ILs, the increase of the ion concentration of the surrounding medium decreased the lamellar distance. The change in the lamellar distance followed the concentration (see Supporting information, Figure S3). These data are comparable to results published by Jing *et al*. (Jing et al., 2016), who studied imidazolium based ILs. 1-hexyl-3-methylimidazolium chloride caused the lamellar distance of α-PC to shrink as a function of IL concentration, with the highest concentration (0.8 M) causing a change of over 1 nm.

A similar effect, although smaller in magnitude, was also observed for supported PC multilayers previously both computationally and by neutron reflectometry (Benedetto et al., 2015; Benedetto et al., 2014). Both techniques showed a decrease in the lamellar distance, but the effect was an order of magnitude smaller compared to the results of Jing et al.: ~0.1 nm for both studied ILs, *i.e.* 1-butyl-3-methylimidazolium chloride and choline chloride. The magnitude of the change in lamellar distance and the effects of increasing concentration are likely due to the different kinetics of liposomal dispersions compared to those of supported multilayers. For example, Amenitsch *et al*. (Amenitsch et al., 2004) measured the effect of lithium chloride concentration on DPPC and POPC MLVs and on supported multilayers and observed that while a significant reduction in bilayer thickness occurred in liposomes exposed to 0.1-0.5 M lithium chloride, lamella in supported stacks actually expanded when exposed to the salt.

Previous works (Benedetto et al., 2015; Benedetto et al., 2014) have attributed the shrinking of the lamella to the absorption of ions into the lipid bilayer. IL cations optimized the contact of the imidazolium group with the lipid head groups and the butyl tail with the lipid hydrocarbon tails. This lead to a change in the orientation of the head group of the lipid and, to preserve the volume of the molecule, shrinkage of the bilayer. In another study (Jing et al., 2016), the increasing SAXS peak height was interpreted to show that amphiphilic ILs enter the lipid bilayer and increase its electronic density. In our data, a similar increase in peak intensity is observed. However, as peak intensity depends on the electron density difference between the scattering structure and the solvent, this does not definitely show that the less harmful ionic liquids penetrate the multilayer. The effects of ILs appear equal throughout the multilayer, as peak width remains virtually constant, corresponding to a constant amount of ordered lamellae. The presence of only one lamellar distance and the similarity of the width and shape of diffraction peaks in the samples treated with ILs to those of the reference sample indicate that lamellar distance and order of the inner lamellae is similar to those of the outer lamellae in all samples. The effect of longer-chained ILs on the lamellar distance was small but consistent: the low concentrations that did not disrupt the lamellar structure of the MLVs caused a slight thinning of the lamellae. However, the concentrations used were low and the lamellar change equally modest. For comparison, the previous SAXS results (Jing et al., 2016) indicate that longer-chain imidazolium-based ILs do not change bilayer thickness.

The effects of the phosphonium-based ILs on the lipid bilayer are not limited to an effect on the *d*-spacing. The increase of the length of the hydrocarbon chain ([P_{14444}][OAc]) and especially the increase in the length of the sidechains ([P_{8881}][OAc]) resulted in a completely destroyed lamellar structure.

3.2 Large unilamellar vesicles

3.2.1 Effects of [P_{14444}][OAc] and [P_{14444}][Cl] on LUVs

The effects of [P_{14444}][OAc] and [P_{14444}][Cl] on large unilamellar vesicles composed of eggPC, eggPG and cholesterol were studied by DLS and zeta potential measurements. The zeta potentials of the reference LUVs were negative, until a sudden reversal at an IL concentration of 0.1 mM. DLS results showed that the diameter of the LUVs decreased with increasing concentration. At a concentration of 1 mM, aggregation of the sample was observed (Table 2 and Supporting information, Figure S5), indicating formation of novel IL-phospholipid structures.

The reversal of the surface charge of the liposomes indicates that the LUVs are coated with IL cations. However, the SAXS pattern of the liposomes remains unchanged at a concentration of 0.4 mM [P_{14444}][OAc]

and $[P_{14444}][Cl]$. For comparison, at higher (3 mM) concentration, the SAXS patterns clearly differ from the reference, indicating a change in the structure of the lipid bilayer (See Supporting information, Figure S6-S7). For [emim][OAc], this kind of a change was not observed (see Supporting information, Section 5.2), *i.e.* for eggPC/eggPC/cholesterol vesicles exposed to [emim][OAc], no significant changes in the zeta potential or the SAXS pattern were detected.

Table 2: The effect of anion size of $[P_{14444}]^+$ on eggPC/eggPG/cholesterol LUV size and zeta potential from DLS measurements. Z-average (corresponding to diameter) and zeta potential (ζ) as a function of $[P_{14444}]OAc$ and $[P_{14444}]Cl$ concentration (c). Average and standard deviation of three consecutive measurements. Values marked with asterisks indicate measurements from an aggregating sample.

c (mM)	$[P_{14444}]OAc$			$[P_{14444}]Cl$		
	Z-average (nm)	ζ (mV)	PDI	Z-average (nm)	ζ (mV)	PDI
0	146 ± 2	-60 ± 1	0.3	145 ± 3	-63 ± 1	0.23
0.0001	141 ± 2	-57 ± 1	0.36	151 ± 3	-68 ± 2	0.24
0.001	137 ± 2	-59 ± 2	0.36	129 ± 3	-73 ± 5	0.14
0.01	137 ± 3	-60 ± 2	0.37	126 ± 1	-64 ± 1	0.16
0.1	124 ± 2	50 ± 1	0.35	119 ± 1	55 ± 1	0.17
1	160 ± 12*	-	0.49	208 ± 40*	-	0.42

3.2.2 Effects of $[P_{8881}][OAc]$ on LUVs

In DLS and zeta potential measurements, eggPC/eggPG and eggPC/eggPG/cholesterol liposomes displayed changes after interacting with $[P_{8881}][OAc]$. Similarly as with the other ILs, the liposomes shrunk upon addition of the IL based on the DLS results. The zeta potential of the liposomes changed to positive already at 0.05 mM concentration (Table 3). However, the liposomes were disrupted at different concentrations based on the DLS results: liposomes containing cholesterol could withstand up to 0.5 mM $[P_{8881}][OAc]$, while the liposomes lacking cholesterol began to dissolve at 0.1 mM IL concentration. This is consistent with the notion that cholesterol stiffens and stabilizes the bilayer.

The SAXS results showed markedly different effects of $[P_{8881}][OAc]$ on the two kinds of LUVs. At low concentration (0.8 mM), the IL affected the bilayer of eggPC/eggPG liposomes little (see Supporting information, Figure S9). Thus, a bilayer-like structure seems to be still intact in the sample at this concentration, even though the vesicle has been disrupted. The highest concentration studied, *i.e.* 17 mM, destroyed the characteristics referring to a lipid bilayer completely, thus indicating a high disorder. However, based on the SAXS results, the lipid bilayers in eggPC/eggPG/cholesterol LUVs are very sensitive to the addition of $[P_{8881}][OAc]$ even at low concentration (0.8 mM). An effect not seen with any other surveyed IL occurred: the appearance of well-defined diffraction peaks (Figure 3). At 0.8 mM concentration, $[P_{8881}][OAc]$ evidently separated the lipid species in liposomes containing cholesterol. These diffraction peaks were not

observed at higher IL concentrations, where the scattering patterns indicate that a defined lipid bilayer is lost. At these higher concentrations, results for liposomes containing and lacking cholesterol are similar.

Table 3: DLS measurements of the Z-average (related to diameter) and zeta potential (ζ) of eggPC/eggPG/cholesterol and eggPC/eggPG LUVs upon addition of [P_{8881}][OAc] as a function of IL concentration. Average and standard deviation of three consecutive measurements. Values marked with asterisks indicate measurements from an aggregating sample.

c (mM)	eggPC/eggPG/cholesterol			eggPC/eggPG		
	Z-average (nm)	ζ (mV)	PDI	Z-average (nm)	ζ (mV)	PDI
0	135 ± 2	-42 ± 4	0.37	142 ± 2	-75 ± 1	0.13
0.05	125 ± 1	45 ± 2	0.30	131 ± 3	51 ± 1	0.14
0.1	104 ± 1	47 ± 2	0.20	154 ± 7*	-	0.22
0.2	101 ± 1	56 ± 2	0.15	-	-	
0.5	111 ± 1	60 ± 4	0.22	-	-	
0.8	212 ± 30*	-	0.28	-	-	

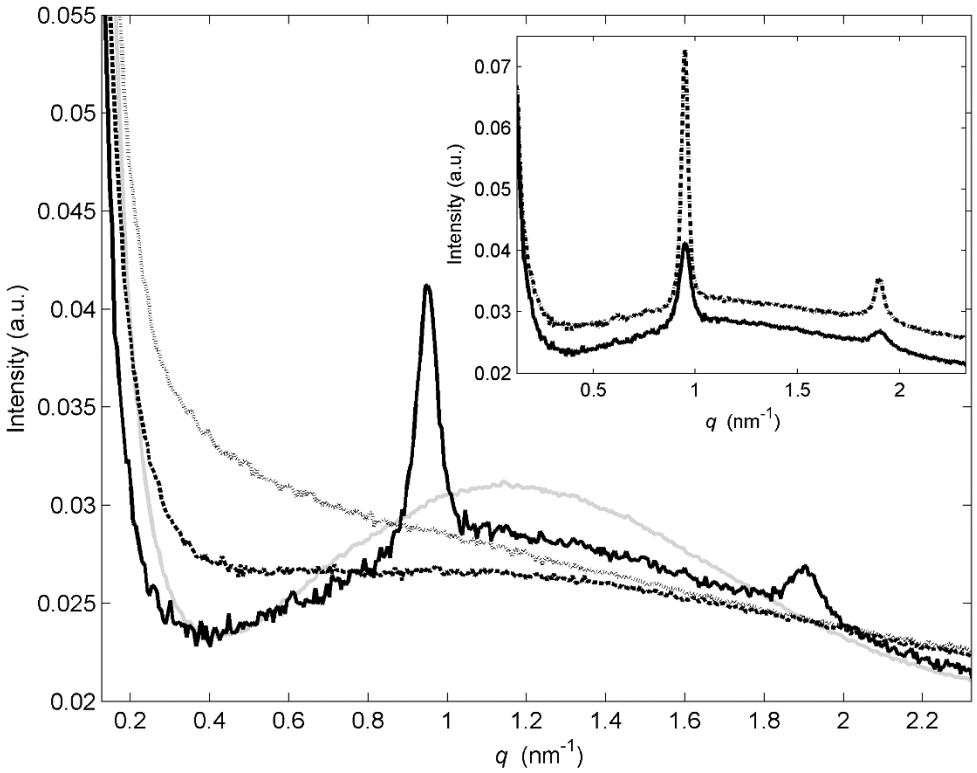

Figure 3. SAXS patterns of eggPC/eggPG/cholesterol LUVs exposed to [P_{8881}][OAc]. Reference LUVs (light gray) and LUVs exposed to 0.8 mM, 8 mM, and 17 mM [P_{8881}][OAc] (black solid, black dashed and dark grey line, respectively). Insert: Scattering pattern of LUVs exposed to 0.8 mM [P_{8881}][OAc] at 20 minutes (solid line) and 30 minutes (dashed line) after IL addition. Curves are shifted vertically for clarity.

The diffraction peaks of eggPC/eggPG/cholesterol in combination with 0.8 mM [P_{8881}][OAc] do not coincide with the diffraction peaks of pure POPC in the MLV samples discussed above. Pure POPC and eggPC MLV have diffraction peaks in the same position (see Supporting information, Figure S8) in spite of the variation in the lengths of the hydrocarbon tails of the latter. The lattice distance of the new structure is 6.6 nm, which is only slightly larger than that of POPC MLV. Addition of even 1 mol% of a charged lipid causes the diffraction peaks of POPC/POPG MLV to disappear (Supporting information, Figure S10). Pure eggPG MLVs do not form a coherently scattering lamellar structure in aqueous solution due to the repulsive forces of the charged head groups. Cholesterol, on its own, does form ordered structures, but the lamellar distance is radically smaller than that of eggPC (see Supporting Information, Figure S11). As cholesterol is not soluble in water at the used concentration, even with the addition of [P_{8881}][OAc], it seems unlikely that cholesterol is the source of the diffraction. The most likely source of these lamellar peaks is thus the separation of eggPC from the rest of the lipid bilayer.

Curiously, where the same IL concentration in POPC MLVs lowered the peaks and induced disorder over time, the order in the lamellae appearing in the eggPC/eggPG/cholesterol sample grew during the measurement (Figure 3 insert). Also, the same concentration of [P_{8881}][OAc] with LUV without cholesterol did not induce a similar radical change (Supporting information, Figure S9). Thus, it can be concluded that the presence of cholesterol in the membrane is needed for this separation and stacking to occur. The concentration of [P_{8881}][OAc] (0.8 mM) matches that of cholesterol (20 mol% of lipids, 0.8 mM). The concentration of eggPC in the sample with cholesterol is lower (60 mol% of lipids) than in the sample without cholesterol (80 mol%), so this effect is not due to excess of eggPC in the sample. The separation may be due to a matching concentration of the negatively charged lipid, the positively charged, flexible IL cation and the small but stiff cholesterol molecules, which likely aggregate, allowing the zwitterionic eggPC to aggregate separately into multilamellar structures.

The order in the lamellae grows during the measurement, which is evidenced both by the increasing intensity of the lamellar peaks and the narrowing of the peaks. Based on the changes in the FWHM of the peaks, the lower limit for the size of the scattering domain increases from 150 nm to 240 nm (calculated with Equation 1). The scattering domain at the end of the measurement is thus significantly larger than that of reference POPC MLVs.

Recent results indicate a reorganization of an α-PC membrane when exposed to imidazolium-based ILs with varying hydrocarbon chain lengths (Yoo et al., 2016). Supported α-PC membranes underwent morphological changes, and multilayer structures appeared at 0.1-20 mM IL concentration, depending on the cation. This was attributed to ILs inducing a bending and destabilisation of the lipid bilayer. An appearance of multilayer

structures from an unilamellar system is thus not without precedent, but the clear sorting effect induced by the lowest studied concentration of [P_{8881}][OAc] observed only with cholesterol-containing liposomes is likely due to a different mechanism.

The effects of [P_{8881}][OAc] depend both on its concentration and liposome composition. For MLVs, the well-ordered structure starts disappearing at c = 0.8 mM. At this concentration, the eggPC/eggPG LUV sample retains its bilayer structure, even though the liposomes have aggregated, and the eggPC/eggPG LUV are separated into large aggregates, parts of which are well ordered. A higher concentration (8 mM) eliminates the remnants of the bilayer structure in all the samples, but an even higher concentration (17 mM) induces a new structure in the sample that contains pure POPC MLVs, but this does not occur in the eggPC/eggPG or eggPC/eggPC/cholesterol LUV samples. The results suggest that the new induced structures are linked to the presence of phosphatidylcholine in the sample, and are highly dependent on the age of the sample and the experimental conditions.

SAXS has previously been applied to studies of the electron density of lipid bilayers, giving insight into the structure of these complex systems. However, SAXS studies of the effect of ILs are still rare. In our studies, the measurement times for dilute solutions were in the order of minutes, but the millisecond resolution of high-brilliance beamlines opens up the possibility for future studies to truly follow the dynamics of the bilayer in real time, and a systematic mapping of the self-assembled structures that arise in certain conditions is warranted.

4 Conclusions

Many previous studies indicate that phosphonium-based ILs are more harmful than other moieties, but the precise toxicity mechanism remains elusive. However, it is clear that interactions with the lipids in the cell membrane are important pathways for toxicity. Our results provide insight into these interactions. In MLVs, the lamellar distance of the vesicles decreases with increasing IL concentration. This relationship appears to hold for several less harmful IL concentrations and species and it is independent of the IL cation type. The thinning of the lamellar distance is naturally limited to IL varieties and concentrations which do not disrupt the vesicles. However, it is clear that even these ILs pass through the multilayer structure.

The zeta potential of the studied anionic LUVs appears largely unaffected by the IL concentration until, at certain concentration, it is suddenly reversed to a highly positive value, indicating that the liposome surfaces are covered by IL cations. When the concentration is still increased, the vesicles aggregate, likely forming novel IL-phospholipid structures. At concentrations which disrupt the LUVs, the ILs destroy the lamellar

structure of MLVs. For LUVs, the DLS results show that an increase in IL concentration leads to a slight decrease in vesicle size.

Cholesterol has usually been thought to strengthen the lipid bilayer against external agents both by inducing order in acyl chains and by assembling into cholesterol rafts. Inclusion of cholesterol in LUVs showed this protective effect also against [P_{8881}][OAc]. The IL ruptured LUVs without cholesterol at lower concentrations than LUVs with cholesterol, but at concentration exceeding this, effects on the cholesterol-containing liposomes were more severe, as evidenced by SAXS. The ruptured liposomes reassembled into organized lamellae, indicating that at this concentration [P_{8881}][OAc] has the ability to separate the lipid species, but only when cholesterol is present in the lipid bilayer. Our results show that under certain conditions, phosphonium-based ionic liquids have the ability to create new self-assembled structures from phospholipids.

Acknowledgements

The research leading to these results has received funding from the European Community's Seventh Framework Program (FP7/2007-2013) CALIPSO under grant agreement nº 312284. Financial support from the Magnus Ehrnrooth Foundation (S.K.W.) and the Academy of Finland projects 266342 and 276075 (S.K.W) are gratefully acknowledged. Dr. Christopher Söderberg is acknowledged for support during beam time, Dr. Ulla Vainio for discussions about the SAXS measurements, Harry Ahlgren for assistance with the DLS and zeta potential measurements, and Jesper Långbacka for assistance with the CMC measurements.

References

Amenitsch, H., Rappolt, M., Teixeira, C.V., Majerowicz, M., Laggner, P., 2004. In situ sensing of salinity in oriented lipid multilayers by surface X-ray scattering. Langmuir 20, 4621-4628.

Antonietti, M., Kuang, D., Smarsly, B., Zhou, Y., 2004. Ionic Liquids for the Convenient Synthesis of Functional Nanoparticles and Other Inorganic Nanostructures. Angewandte Chemie International Edition 43, 4988-4992.

Benedetto, A., Ballone, P., 2015. Room temperature ionic liquids interacting with bio-molecules: an overview of experimental and computational studies. Philosophical Magazine, 1-25.

Benedetto, A., Bingham, R.J., Ballone, P., 2015. Structure and dynamics of POPC bilayers in water solutions of room temperature ionic liquids. J Chem Phys 142, 124706-.

Benedetto, A., Heinrich, F., Gonzalez, M.A., Fragneto, G., Watkins, E., Ballone, P., 2014. Structure and Stability of Phospholipid Bilayers Hydrated by a Room-Temperature Ionic Liquid/Water Solution: A Neutron Reflectometry Study. J Phys Chem B 118, 12192-12206.

Blesic, M., Marques, M.H., Plechkova, N.V., Seddon, K.R., Rebelo, L.P.N., Lopes, A., 2007. Self-aggregation of ionic liquids: micelle formation in aqueous solution. Green Chem 9, 481-490.

Chen, S., Zhang, S., Liu, X., Wang, J., Wang, J., Dong, K., Sun, J., Xu, B., 2014. Ionic liquid clusters: structure, formation mechanism, and effect on the behavior of ionic liquids. Phys Chem Chem Phys 16, 5893-5906.

Cromie, S.R.T., Del Popolo, M.G., Ballone, P., 2009. Interaction of Room Temperature Ionic Liquid Solutions with a Cholesterol Bilayer. J Phys Chem B 113, 11642-11648.
Diaz, M., Ortiz, A., Ortiz, I., 2014. Progress in the use of ionic liquids as electrolyte membranes in fuel cells. J Membrane Sci 469, 379-396.
Docherty, K.M., Kulpa, C.F., 2005. Toxicity and antimicrobial activity of imidazolium and pyridinium ionic liquids. Green Chem 7, 185-189.
Dusa, F., Ruokonen, S.K., Petrovaj, J., Viitala, T., Wiedmer, S.K., 2015. Ionic liquids affect the adsorption of liposomes onto cationic polyelectrolyte coated silica evidenced by quartz crystal microbalance. Colloid Surface B 136, 496-505.
Earle, M.J., Seddon, K.R., 2000. Ionic liquids. Green solvents for the future. Pure Appl Chem 72, 1391-1398.
Egorova, K.S., Ananikov, V.P., 2014. Toxicity of Ionic Liquids: Eco(cyto)activity as Complicated, but Unavoidable Parameter for Task-Specific Optimization. Chemsuschem 7, 336-360.
Fraser, K.J., MacFarlane, D.R., 2009. Phosphonium-Based Ionic Liquids: An Overview. Aust J Chem 62, 309-321.
Gaynor, P.M., Zhang, W.Y., Salehizadeh, B., Pettiford, B., Kruth, H.S., 1996. Cholesterol accumulation in human cornea: evidence that extracellular cholesteryl ester-rich lipid particles deposit independently of foam cells. Journal of lipid research 37, 1849-1861.
Holding, A.J., Heikkila, M., Kilpelainen, I., King, A.W.T., 2014. Amphiphilic and Phase-Separable Ionic Liquids for Biomass Processing. Chemsuschem 7, 1422-1434.
Jing, B., Lan, N., Qiu, J., Zhu, Y., 2016. Interaction of Ionic Liquids with Lipid Bilayer: A Biophysical Study of Ionic Liquid Cytotoxicity. The Journal of Physical Chemistry B.
Labafzadeh, S.R., Helminen, K.J., Kilpelainen, I., King, A.W.T., 2015. Synthesis of Cellulose Methylcarbonate in Ionic Liquids using Dimethylcarbonate. Chemsuschem 8, 77-81.
Labrador, A., Cerenius, Y., Svensson, C., Theodor, K., Plivelic, T., 2013. The yellow mini-hutch for SAXS experiments at MAX IV Laboratory. J Phys Conf Ser 425.
Lemmich, J., Mortensen, K., Ipsen, J.H., Honger, T., Bauer, R., Mouritsen, O.G., 1997. The effect of cholesterol in small amounts on lipid bilayer softness in the region of the main phase transition. Eur Biophys J Biophy 25, 293-304.
Mannock, D.A., Lewis, R.N.A.H., McMullen, T.P.W., McElhaney, R.N., 2010. The effect of variations in phospholipid and sterol structure on the nature of lipid-sterol interactions in lipid bilayer model membranes. Chem Phys Lipids 163, 403-448.
Mikkola, S.K., Robciuc, A., Lokajova, J., Holding, A.J., Lammerhofer, M., Kilpelainen, I., Holopainen, J.M., King, A.W.T., Wiedmer, S.K., 2015. Impact of Amphiphilic Biomass-Dissolving Ionic Liquids on Biological Cells and Liposomes. Environ Sci Technol 49, 1870-1878.
Mills, T.T., Tristram-Nagle, S., Heberle, F.A., Morales, N.F., Zhao, J., Wu, J., Toombes, G.E.S., Nagle, J.F., Feigenson, G.W., 2008. Liquid-liquid domains in bilayers detected by wide angle x-ray scattering. Biophys J 95, 682-690.
Pabst, G., Kucerka, N., Nieh, M.P., Rheinstadter, M.C., Katsaras, J., 2010. Applications of neutron and X-ray scattering to the study of biologically relevant model membranes. Chem Phys Lipids 163, 460-479.
Petkovic, M., Ferguson, J.L., Gunaratne, H.Q.N., Ferreira, R., Leitao, M.C., Seddon, K.R., Rebelo, L.P.N., Pereira, C.S., 2010. Novel biocompatible cholinium-based ionic liquids-toxicity and biodegradability. Green Chem 12, 643-649.
Pretti, C., Chiappe, C., Baldetti, I., Brunini, S., Monni, G., Intorre, L., 2009. Acute toxicity of ionic liquids for three freshwater organisms: Pseudokirchneriella subcapitata, Daphnia magna and Danio rerio. Ecotox Environ Safe 72, 1170-1176.
Ranke, J., Müller, A., Bottin-Weber, U., Stock, F., Stolte, S., Arning, J., Störmann, R., Jastorff, B., 2007. Lipophilicity parameters for ionic liquid cations and their correlation to in vitro cytotoxicity. Ecotox Environ Safe 67, 430-438.
Ruokonen, S.-K., Sanwald, C., Sundvik, M., Polnick, S., Vyavaharkar, K., Duša, F., Holding, A.J., King, A.W.T., Kilpeläinen, I.A., Lämmerhofer, M., Panula, P., Wiedmer, S.K., 2016. Effect of ionic liquids on zebrafish (Danio rerio) viability, behavior, and histology; correlation between toxicity and ionic liquid aggregation. Environ Sci Technol.

Stolte, S., Arning, J., Bottin-Weber, U., Muller, A., Pitner, W.R., Welz-Biermann, U., Jastorff, B., Ranke, J., 2007. Effects of different head groups and functionalised side chains on the cytotoxicity of ionic liquids. Green Chem 9, 760-767.

Thi, P.T.P., Cho, C.W., Yun, Y.S., 2010. Environmental fate and toxicity of ionic liquids: A review. Water Res 44, 352-372.

Varga, Z., Wacha, A., Bota, A., 2014. Osmotic shrinkage of sterically stabilized liposomes as revealed by time-resolved small-angle X-ray scattering. J Appl Crystallogr 47, 35-40.

Yoo, B., Jing, B., Jones, S.E., Lamberti, G.A., Zhu, Y., Shah, J.K., Maginn, E.J., 2016. Molecular mechanisms of ionic liquid cytotoxicity probed by an integrated experimental and computational approach. Sci Rep-Uk 6, 19889.

Zhu, S.D., Wu, Y.X., Chen, Q.M., Yu, Z.N., Wang, C.W., Jin, S.W., Ding, Y.G., Wu, G., 2006. Dissolution of cellulose with ionic liquids and its application: a mini-review. Green Chem 8, 325-327.